Sensors and Actuators B 223 (2016) 138–148

Contents lists available at ScienceDirect

Sensors and Actuators B: Chemical

journal homepage: www.elsevier.com/locate/snb

A novel organic pollutants gas sensing material p-type $CuAlO_2$ microsphere constituted of nanoparticles for environmental remediation

S. Thirumalairajan*, Valmor R. Mastelaro

Instituto de Física de São Carlos (IFSC), University de São Paulo, CP 369, 13560-970 São Carlos, SP, Brazil

ARTICLE INFO

Article history:
Received 11 August 2015
Received in revised form 9 September 2015
Accepted 18 September 2015
Available online 21 September 2015

Keywords:
$CuAlO_2$
Hydrothermal
Self assembly
Microspheres
Toxic gas
XAS

ABSTRACT

In this paper, novel organic pollutants gas sensing material $CuAlO_2$ microspheres constituted of nanoparticles were successfully prepared by wet chemical route and characterized by structural (XRD, XAS), morphological (SEM, TEM, HRTEM) and thermal (TG) analysis. In addition, the oxidation (O_3 and NO_2) and reduction (NH_3 and CO) toxic gas sensing properties of the prepared $CuAlO_2$ microspheres were systematically investigated. $CuAlO_2$ microspheres exhibited real-time response for very low detection level of 200 ppb at 200 °C, with fast response (29 s), recovery (45 s) time, good reproducibility and stability to ozone gas indicating their promising application in toxic gas sensor which is better than other oxidation and reduction gases. Also comparative studies of charge-transport properties mainly ascribed to the increased proportion of ozone gas exposed surface active layers are discussed in gas sensing mechanism.

1. Introduction

Controlled size and shape dependent properties of nanomaterials have been extensively studied with the aim of enhancing the performance of toxic gas sensors for environmental remediation [1]. In recent years researchers have found that transparent conducting oxide (TCO) nanomaterials are presenting themselves as one of the most important class of materials due to their excellent exclusive properties of low electrical resistivity and high optical transparency in the visible range [2–4]. The synthesis of nanosized TCO materials with controlled morphology and texture has attracted intensive interest since these parameters play an important role in determining their optical, electrical, catalytic, and sensing properties [5]. More importantly, this type of materials might possess new physicochemical properties arising from their secondary architecture [6]. Delafossite compounds belong to a family of ternary oxides with the general formula $A^{1+}B^{3+}O_2$. In this structure, the A cation is linearly coordinated to two oxygen ions and occupied by metals such as Pd, Pt, Cu or Ag. The inter-atomic distance between cations is quite small, ranging from 2.8 to 3.0 Å for most compounds [7]. The B cation (Fe, Al and Ga) is located in distorted edge-shared BO_6 octahedral with a central metal cation. The universality of the toxic gas sensing performance of $CuBO_2$ has attracted extensive interest and attention during the last decade [8]. Recently, $CuCrO_2$ has been applied for room temperature ozone sensor, unfortunately, for the ozone concentration of 20–50 ppm the response was very poor [9]. The design and development of highly toxic gas sensing delafossite type materials with low detection level (ppb) has been a challenging research subject in the field of materials science [10]. $CuAlO_2$ is one of the p-type delafossite-type oxide having high electrical conductivity and exhibits good oxidation–reduction characteristics at wide temperature and good matched properties for sensing and catalysis behaviour. Hence, $CuAlO_2$ was chosen as a sensing material to sense different toxic gases in the present work.

Several solution routes and gas phase evaporation techniques have been developed for the preparation of $CuAlO_2$ materials [11,12]. However, most of the reported routes were related to a complex reaction process. The hard template, high-temperature and high-pressure were usually used to control the morphology of the final product, which are not beneficial for obtaining high-purity and low defect density products [13]. Among the various methods, hydrothermal method is an environmental facile dominant tool for the synthesis of nanoscale materials [14–16]. Significant advantages of this method are controlled size, low temperature growth, cost effectiveness and less complicated. In addition, polyvinyl

* Corresponding author.
E-mail address: sthirumalairajan@gmail.com (S. Thirumalairajan).

http://dx.doi.org/10.1016/j.snb.2015.09.092
0925-4005/

alcohol (PVA) is a common and good chelating agent for metal ions to form coordination complexes. Metal nitrate ion and PVA ion coordination complex can easily be synthesized by hydrothermal reaction. Recently, $CuAlO_2$ nanoparticles having size in the range <100 nm, but with no interesting morphology were prepared using wet chemical methods [17,18]. In addition, the morphology and structure of $CuAlO_2$ material is the key factor in influencing the performance and enhancing the gas-sensing properties.

The toxic gas sensor detection is very important because many gases are harmful to organic life. In particular, detection of ozone (O_3) is currently the subject of extensive scientific and technological research, motivated by its deleterious impact on the environment and on human health and safety [19]. Recently, transparent conducting oxide based toxic gas sensors are used for environmental monitoring and industrial applications due to their advantages such as small dimensions, low cost and convenient operation [20,21]. Commercially available gas sensors which normally operate in the range of temperatures between 100 and 400 °C are made mainly of semiconductor based materials used for the detection of gaseous species down to several parts per million (ppm) [22]. There is a great demand to enhance the sensitivity of chemical sensors for various sensing applications such as monitoring and conditioning of air quality, detection of flammable or toxic gases, medical diagnosis, there emerges a strong motivation to develop sensors which are capable of sensing gas concentration changes down to several parts per billion (ppb) [23]. Therefore toxic gas sensor with good sensitivity, detection limit, fast response and recovery time are urgently required. To the best of our knowledge reports on oxidization and reduction gas sensing by microsphere constituted of $CuAlO_2$ nanoparticles is not available in the open literature.

In this article, we report for the first time the shape controlled synthesis of microsphere constituted of $CuAlO_2$ nanoparticles via a facile one stop hydrothermal route. The morphology can be controlled by merely changing the hydrothermal reaction and calcination time. The prepared $CuAlO_2$ morphology was used for fabricating toxic gas sensor device. We detected oxidation gases (O_3 and NO_2) and reduction gases (NH_3 and CO) at various concentrations in order to obtain a relation between the sensor response and the working temperature of all these gases. Finally, comparative studies of charge-transport properties mainly ascribed to the increased proportion of exposed surface active layers and gas molecules are discussed in gas sensing mechanism.

2. Experimental

2.1. Materials

Copper (II) nitrate trihydrate (Cu $(NO_3)_2{\cdot}3H_2O$), aluminium nitrate nonhydrate (Al $(NO_3)_2{\cdot}9H_2O$), polyvinyl alcohol (PVA), ethylene glycol (EC) and sodium hydroxides (NaOH) were used in the present experiment. All chemicals purchased were of analytical pure grade and used without further purification.

2.2. Synthesis of microspheres constituted of $CuAlO_2$ nanoparticles

In a typical hydrothermal method, 0.1 mol of $Cu(NO_3)_2{\cdot}3H_2O$ and 0.12 mol of $Al(NO_3)_2{\cdot}9H_2O$ precursors were dissolved in 50 mL of distilled water, followed by the addition of 0.2 mol surfactant PVA dissolved in 25 mL double distilled water with magnetic stirring, along with the addition of 5 mL EG and 2 g NaOH as a mineralizar to form homogeneous blue coloured solution, which was then transferred into a 110 mL Teflon autoclave. The autoclave was sealed and maintained at 200 °C for 24 h. After cooling down to room temperature naturally, the obtained products were filtered by centrifugation and washed several times with distilled water and anhydrous ethanol. The products were dried in an oven at 80 °C for 12 h. Finally, the powder was calcinated at different time (0.5, 1, 2, 4 and 5 h) for 1100 °C to obtain $CuAlO_2$ powder and used for further characterization.

2.3. Characterization analysis

The crystal phase and purity of the prepared $CuAlO_2$ samples were identified by X-ray powder diffraction (XRD), CuKα1 radiation (K = 1.5406 Å, Rigaku diffractometer, model DMax-2500 PC) in the 2θ range from 20 to 80 °C. The thermal stability was investigated using a thermogravimetric analyzer (Diamond TG/DTA, PerkinElmer Instruments). Scanning electron microscopy (SEM) measurements were carried out on a F50 INSPECT scanning microscope to investigate the morphology and surface structure of the samples. Transmission electron microscopy (TEM) and high-resolution transmission electron microscopy (HRTEM) images were recorded on a TECNAI F20 microscopy at an acceleration voltage of 200 kV. A trace amount of the sample was suspended in ethanol solution followed by sonication for 10 min. Carbon-coated copper grids were used as the sample holders. Cu K-edge X-ray absorption spectra were collected at the LNLS (National Synchrotron Light Laboratory) facility using the D04B-XAS2 beam line. The LNLS storage ring was operated at 1.36 GeV and 100–160 mA. X-ray absorption spectra were collected at the Cu K-edge (8979 eV) in transmission mode using an Si(1 1 1) monochromator. All the XAFS data were collected at room temperature. X-ray absorption near edge structure (XANES) spectra at the Cu K-edge were record between 8920 and 9100 eV using an energy step of 0.3 eV around the edge. To provide good energy reproducibility during the XANES data collection, the energy calibration of the monochromator was checked during the collection of the sample data using a Cu metal foil. The Cu K-edge extended X-ray absorption fine structure (EXAFS) spectra were collected between 8890 and 9800 eV using an energy step of 2.0 eV. The XANES normalization and the extraction of EXAFS spectra were performed using the multi-platform applications for X-ray absorption (MAX) software package [24].

2.4. Fabrication of $CuAlO_2$ sensing film and detection of various gases

Microspheres constituted of $CuAlO_2$ nanoparticle powders (10 mg) were dispersed in 1 mL isopropyl alcohol by an ultrasonic cleaner for 30 min and the suspension was dropped onto a Si/SiO_2 substrate containing 100 nm thick Pt electrodes separated by a distance of 50 μm. The substrates were then heated to 90 °C for 10 min to evaporate the solvent, followed by calcination at 500 °C for 3 h in an electric furnace in air to stabilize the sample before the gas sensing measurements were performed. The sensor sample was inserted into a test chamber at controlled temperature under different gases like O_3, CO, NO_2 and NH_3. The electrical resistance was measured using Keithley (model 6514) electrometer at an applied dc voltage of 1 V. The sensing response (S) of p-type materials for oxidation gas (O_3 and NO_2) is defined as $S = R_{air}/R_{gas}$, and for reduction gas (CO and NH_3) $S = R_{gas}/R_{air}$. Here electric resistance of the sensor is exposed to the resistance in the air (R_{air}) and to the target oxidizing or reduction gas (R_{gas}). The response time of the sensor is defined as the time required for a change in the electrical resistance to reach 90% of the initial value when exposed to ozone gas. Similarly, the time required for the electrical resistance of the sensor to reach 90% of the initial value after the ozone gas has been turned off is the recovery time. During the measurements the humidity was under controlled condition within the range 50–60% RH.

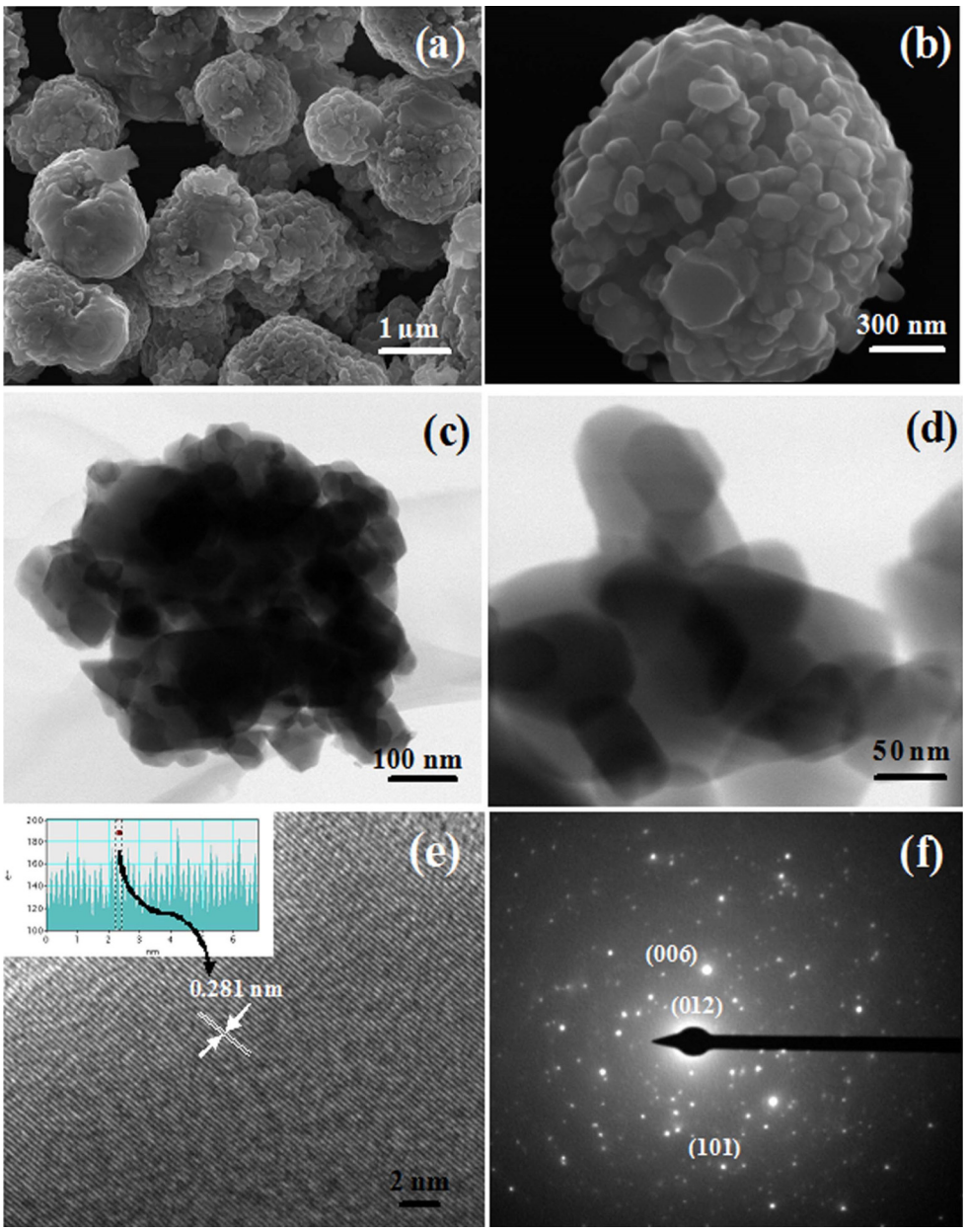

Fig. 1. SEM image of (a) low-magnification, (b) high-magnification, (c) TEM image of low-magnification, (d) high-magnification, (e) HRTEM and (f) SAED pattern of $CuAlO_2$ microspheres constituted of nanoparticles at 1100 °C for 5 h.

3. Results and discussion

3.1. Morphological analysis of $CuAlO_2$ products

A scanning electron microscopy was employed as an effective technique to reveal the surface morphology and structural characters of the resulting products, shown in Fig. 1.

From the SEM images of the $CuAlO_2$ prepared samples obtained through hydrothermal process at 200 °C for 24 h, it can be clearly observed that the samples exhibit microspheres constitute of well structured nanoparticles, as shown in Fig. 1a. The outer surface of the grown morphology clearly presents highly dense packed microsphere shaped morphology. A high magnified examination of these microspheres reveals the additional details of the prepared morphologies. One can see that an individual microsphere is an assembly of many nanoparticles, which can be especially seen from a single microsphere shown in Fig. 1b. The microspheres have an average diameter of 1.5 μm. It should be mentioned that such novel microsphere $CuAlO_2$ morphology has not been reported previously through hydrothermal process.

Further insight into the morphology of $CuAlO_2$ microspheres were gained by using TEM and high-resolution TEM (HRTEM). Fig. 1c displays a typical TEM image of an individual microsphere. The edge portion of the microsphere is lighter than that of the centre and the microstructure consists of $CuAlO_2$ nanoparticles. It is interestingly found that each $CuAlO_2$ nanoparticles assembles to form a dense microstructure (Fig. 1d). The highly porous structure consisting of interconnected nanoparticles with ca. 70 nm diameter is in accordance with the observation in SEM images (Fig. 1b). The typical lattice fringes in the HRTEM image (Fig. 1e) recorded at the tip of the individual $CuAlO_2$ nanoparticles has a single-crystalline nature. The lattice fringe spacing is certified to be 0.282 nm (point between two arrows), corresponding to the lattice interplanar spacing of the crystallographic

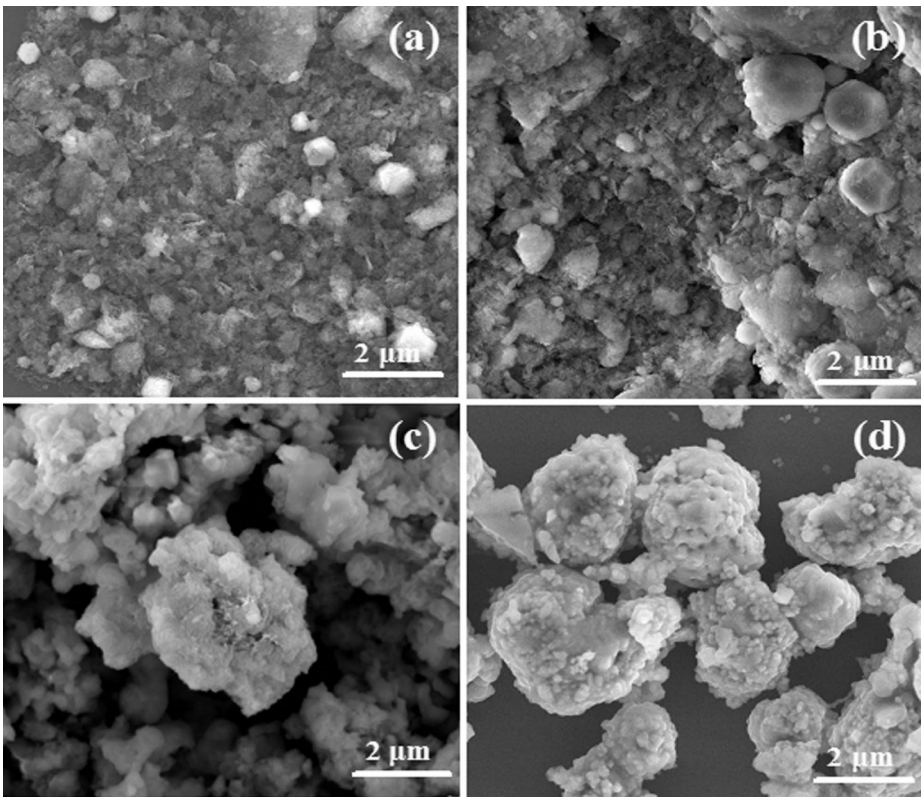

Fig. 2. SEM images of $CuAlO_2$ microspheres constituted of nanoparticles (a) 3 h, (b) 6 h, (c) 12 h and (d) 18 h for 200 °C.

plane (0 1 2) and the preferential growth along the same direction of the structure takes place. By careful checking of many nanoparticles, it is demonstrated that all the $CuAlO_2$ nanoparticles grow along the [0 1 2] direction. In addition, the inter fringe distance was measured to be 0.282 nm based on the measurements of randomly selected 50 fringes, as evident in Fig. 1e (inset top). From the selected area diffraction pattern (SAED), the diffraction rings are observed to be discontinuous and consist of rather sharp spots which indicate good crystallinity of $CuAlO_2$ nanoparticles as shown in Fig. 1f. The major diffraction spots correspond to (0 1 2), (0 0 6) and (1 0 1) diffraction patterns of $CuAlO_2$ structure. No diffraction spots were attributed to the secondary phase, which is in good agreement with the XRD results to be discussed in Section 3.4.

3.2. Impact of time dependent reaction process on the formation of $CuAlO_2$ microspheres

In general, the hydrothermal reaction parameters like temperature, time, and concentration have great effect on the morphology of the resulting products. Our experimental results indicate that the reaction time play a vital role in the formation of final products.

The morphological evolution of $CuAlO_2$ products prepared at different hydrothermal reaction time 3, 6, 12 and 18 h at a constant reaction temperature 200 °C were carefully examined by SEM observation. As shown in Fig. 2a, only agglomerated nanoparticles was observed at early stage of 3 h reaction time, which indicates the microspheres cannot be formed at lesser reaction time and these amorphous particles act as primary particles to form microspheres.

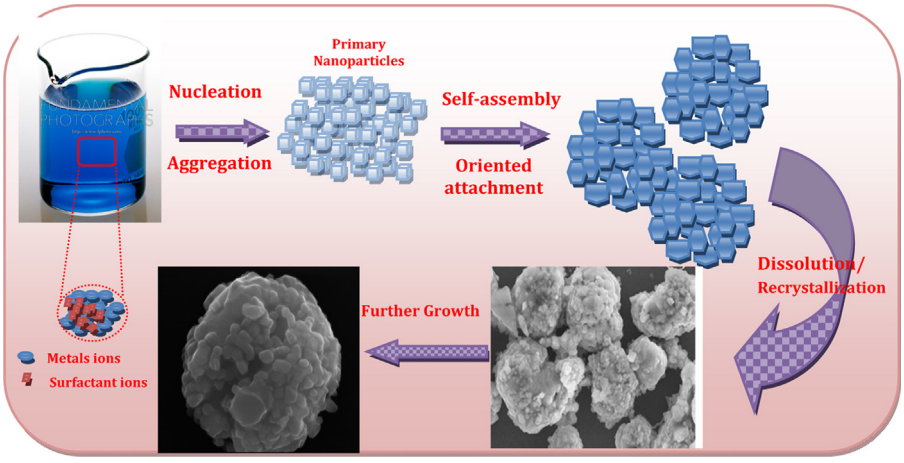

Fig. 3. Schematic illustration of the plausible formation mechanism of $CuAlO_2$ microspheres.

When the reaction time is prolonged to 6 h, nanoparticles are aggregated in large quantities, tending the initial growth of sphere shaped structures as shown in Fig. 2b. Subsequently increasing the reaction time to 12 h, nanoparticles nucleate, aggregate and the shell almost grew into a sphere and more number of nanoparticles sequentially gets attached on to the newly grown microspheres, which is observed in Fig. 2c. Further when the reaction time was increased to 18 h, it can be clearly observed that these microspheres become larger with diameter >2 μm and few aggregated small particles were found on the surface of the microspheres as shown in Fig. 2d. Finally, a clear morphology with well-defined microspheres was formed at 24 h, comprising of secondary $CuAlO_2$ nanoparticles as shown in Fig. 1b. On the basis of above discussion, in the growth process, the reaction time is the most significant controlling factor of the morphology and structure. In the initial process, a group of freestanding crystallites in the reaction solution with unequal shape and size in non-equilibrium state was formed [25]. After the secondary $CuAlO_2$ microspheres were generated, they began to be slowly reduced by surfactant ions, and the surface layer transformed into $CuAlO_2$ nanoparticles. Meanwhile under the synergetic effects of Ostwald ripening and reduction, more $CuAlO_2$ nanoparticles were formed around the original $CuAlO_2$ microspheres in the following reaction process, i.e. to lower the total energy of the system, small crystallites would eventually dissolve into the solution and regrowth the large ones during the reaction time [26]. These facts indicate that the formation of $CuAlO_2$ with microsphere morphology depend on the size of the primary particles. Further, from Fig. 2a–d we observe that both particle size and morphology undergo apparent regular changes with hydrothermal reaction time. The above results indicate that the crystallinity of microspheres increases with increase in hydrothermal reaction time.

3.3. Plausible formation mechanism of microspheres constituted of $CuAlO_2$ nanoparticles

A plausible formation mechanism of the microspheres constituted of $CuAlO_2$ nanoparticles could be presented on the basis of the above mentioned results. Three obvious evolution steps should be involved: (1) nucleation and aggregation, (2) self-assembly by oriented attachment and (3) dissolution and recrystallization as shown in schematic diagram Fig. 3. In the initial hydrothermal reaction stage, metal nitrate ions in the solution react with surfactant ions which aggregate and nucleation to form unstable distorted primary $CuAlO_2$ nanoparticles under supersaturated condition. Secondly, the formed $CuAlO_2$ nanoparticles aggregate together which is driven by the minimization of interfacial energy [27]. The aggregated nanoparticles would act as primary cores that favour the homogenous assembly to produce larger self-assembled aggregates via self-assembly process.

The products undergo an Ostwald ripening process, that is, the larger particles grow at the cost of the smaller ones. This process leads to the formation of compact sphere shape and aggregation speed of nanoparticles from each direction to the core could be same [28]. In the final stage, the dissolution–recrystallization process during the decomposition of the $CuAlO_2$ microspheres leads to the formation of well defined $CuAlO_2$ microspheres under a longer hydrothermal treatment. This result is consistent with the observation that hydrothermal reaction time is a simple and effective way to control the nucleation and growth process and plays a key role in the formation of microspheres constituted of $CuAlO_2$ nanoparticles.

3.4. Structural and thermal analysis

The XRD was used to investigate the changes of the phase structure, purity and crystallite size of the prepared $CuAlO_2$ samples as shown in Fig. 4a To clarify the effect of different calcination time, a series of experiments have been carried out at 1100 °C for 0.5, 1, 2, 4 and 5 h respectively. It can be observed that increasing the calcination time leads to well crystallized $CuAlO_2$ microspheres. The XRD pattern of 0.5 and 1 h samples indicates three crystalline phase mixture like tenorite CuO (*) phase, spinel $CuAl_2O_4$ (#) phase and $CuAlO_2$ with delafossite structure. For 2 and 4 h, a dominant two phase mixture of spinel $CuAl_2O_4$ and delafossite $CuAlO_2$ structure exist, along with a small quantity of CuO. The sharp and narrow diffraction peaks obtained at 1100 °C for 5 h indicate ralatively good crystallinity of sphere shaped morphology. All the diffraction peaks are indexed to the single phase of $CuAlO_2$ with rhombohedral crystal system ($a = b = 2.8584$ Å, $c = 16.9580$ Å, $\alpha = \beta = 90°$, $\gamma = 120°$) of delafossite structure with $R-3m$ space group [29]. No other characteristic peaks arising from any crystal phases were detected in the XRD pattern, indicating that the $CuAlO_2$ samples of high purity could be obtained under 1100 °C calcination temperature maintained for 5 h. No change in the structure was detected by further increasing the calcination time to 6 h. The average crystallite size was estimated by the Debye–Scherrer formula [30] and was found to be ~75 nm. The HRTEM image of microsphere discussed in Section 3.1 shows clear lattice fringes along the growth direction (Fig. 1e). The '*d*' spacing of the lattice fringes was 0.282 nm indexed to the (1 2 1) plane of the $CuAlO_2$ rhombohedral structure.

In addition, the thermal stability process of microspheres constituted of $CuAlO_2$ nanoparticles was performed by thermo gravimetric analysis (TGA) at a heating and cooling rate of

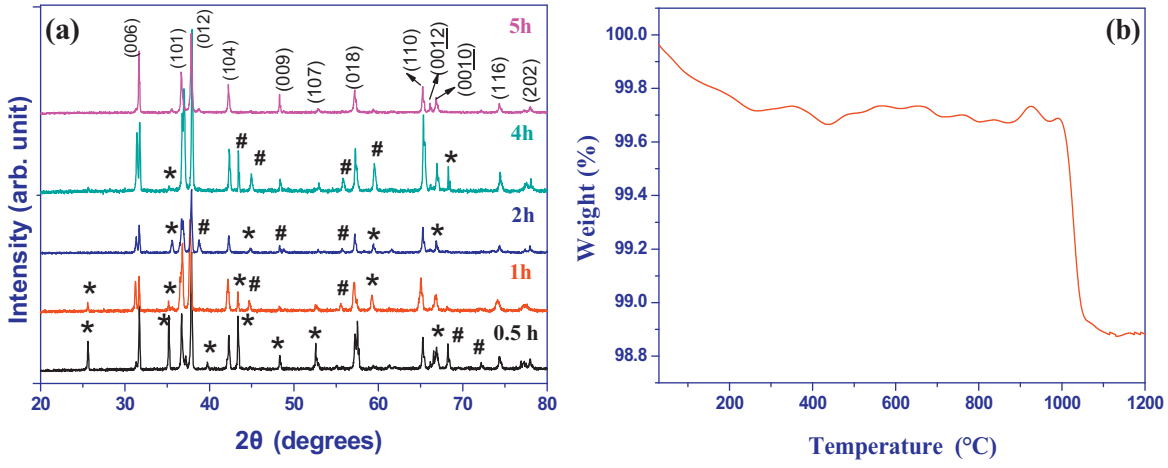

Fig. 4. (a) XRD pattern of the samples with different calcination time and (b) Thermal analysis of $CuAlO_2$ microspheres constituted of nanoparticles at 1100 °C for 5 h.

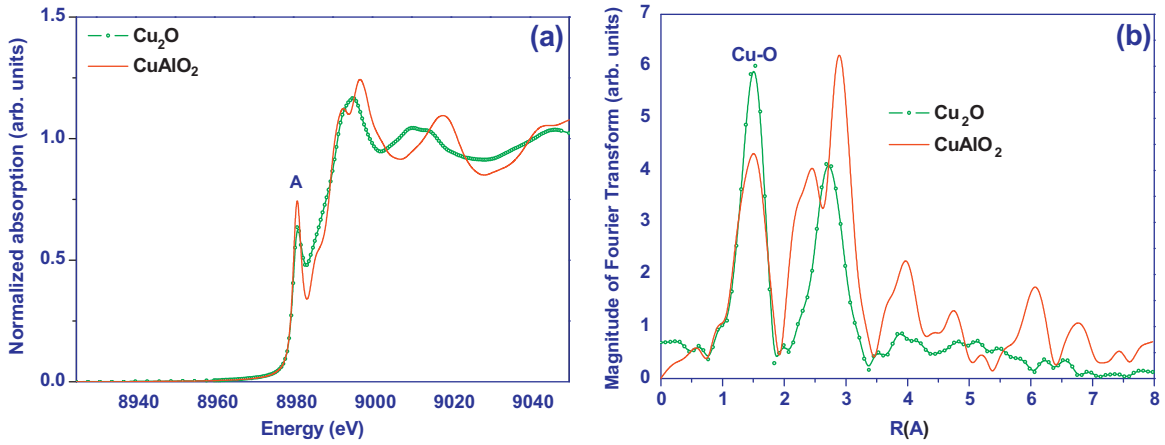

Fig. 5. (a) Cu K-edge XANES spectra, (b) Cu K-edge FT curves of Cu_2O and $CuAlO_2$ samples.

20 °C min^{-1} as shown in Fig. 3. In the first step, ca. 0.3% of mass loss was observed at 230 °C which is attributed to the loss of water molecules or hydroxyl groups. Further, in the entire range of TG curve, the starting weight loss at temperature 230 °C ends at temperature 1050 °C and the total weight loss of approximately 1.1% can be attributed to the mixture of CuO and $CuAl_2O_4$, which is thermodynamically stable at this temperature in air and also due to the presence of more oxygen molecules. This shows that the excess oxygen atom content is 0.14 atoms per unit formula, CuAlO (2 + 0.14) [31]. The excess oxygen atoms in the $CuAlO_2$ sample confirm that the nature of the delafossite compound allows O to exist between the Cu^+ triangle shapes of Cu layers. Excess O influences the contribution of hole carriers in $CuAlO_2$, and O defects play an important role in the p-type structure [32]. The result of TG data shows that the $CuAlO_2$ phase exists in the temperature ranging from 1050 to 1150 °C. The abrupt weight loss occurs at temperature beyond 1100 °C, indicating the melting point behaviour of the $CuAlO_2$ sample. These observations confirm the formation temperature of single phase $CuAlO_2$ microspheres at 1100 °C calcinated for 5 h. The above results indicate that the hydrothermal reaction time and calcination temperature is an important parameter for the formation of clear and well-defined morphology. On comparing the samples prepared with different hydrothermal reaction time and calcination temperature, it can be concluded that the reaction time 200 °C for 24 h and calcination temperature 1100° C for 5 h can be taken as optimized values as shown in Figs. 1b and 4a. Hence, these samples were used for further characterization analysis and for different toxic sensing measurements.

3.5. X-ray absorption spectroscopy of $CuAlO_2$ microspheres

Further, identification and quantification of the different chemical species present in $CuAlO_2$ microsphere sample was performed using X-ray absorption spectroscopy (XAS), an easy, reliable and widely used technique for speciation. While extended X-ray absorption fine structure (EXAFS) can be used to determine the local structure around the absorbing atom, *i.e.*, bond distance, coordination number and chemical identity of the elements, the X-ray absorption near edge structure (XANES) can be used to provide information about oxidation state of an excited atom and its coordination symmetry [33].

Fig. 5a shows the XANES spectra of the Cu_2O and $CuAlO_2$ samples. As can be observed, both samples present the edge energy at 8979.6 eV, indicating that Cu atoms in the $CuAlO_2$ are in Cu^{1+} state. The absorption edge of Cu K-edge XANES is assigned to the main 1s to 4p transition. Peak *A* can be ascribed to the transition 1s to 4p*xy*.

In order to determine the local order structure around Cu atoms in $CuAlO_2$ compound, the EXAFS spectra of Cu_2O (reference compound) and microsphere $CuAlO_2$ sample were also collected. Fig. 5b shows the Fourier transform (FT) magnitude of both samples and as can be observed, the position of the FT first peak of both samples coincide, meaning that Cu—O mean bond length on the first coordination shell in both samples are similar. However, the peak intensities are very different. Concerning the difference in FT peaks located at greater distances, it can be attributed to the difference on the structure of the two samples and also the presence of Al atoms in the $CuAlO_2$ compound. Thus, only the first Cu—O coordination shell is analyzed quantitatively.

To determine the Cu—O first shell coordination number, Cu—O mean bond length and the disorder related to the Cu—O interaction, the EXAFS spectra was fitted according to the IXS standard and criteria subcommittees reports. Table 1 shows the fitting results of Cu K edge EXAFS spectra that correspond to the first coordination shell (Cu—O). As can be observed, the Cu—O mean bond length of both samples obtained from EXAFS results are similar to the literature obtained from XRD measurements [34]. The difference observed in the intensity of first peak of FT intensity between the two samples is due to the high degree of disorder (Debye–Waller factor (σ)) in the $CuAlO_2$ compared to the Cu_2O compound. It was observed that the electrical conductivity is of intrinsic origin, not associated to the presence of impurity phases or to the Cu–Al chemical disorder. These results confirmed that the prepared sample $CuAlO_2$ microspheres are single phase delafossite compound.

3.6. Oxiditation and reduction gas sening measurement of p-type $CuAlO_2$ microspheres

The gas-sensing properties are based on the surface reactions between the sensing material and the test gas. Surface area is

Table 1
Fitting results of the first coordination shell of EXAFS spectra collected at the Cu K-edge and Cu—O mean bond-length obtained from XRD.

Sample	*N* (Cu—O)	*R* (Cu—O) Å	σ^2 (Cu—O) Å	QF	R (Cu—O) Å XRD
Cu_2O	1.9 ± 0.2	1.836 ± 0.001	0.003 ± 0.001	1.8	1.845
$CuAlO_2$	1.9 ± 0.3	1.855 ± 0.002	0.004 ± 0.001	1.8	1.861

N = first shell neighbour number, *R* = Cu—O mean bond-length, σ = Debye–Waller factor. QF = quality factor.

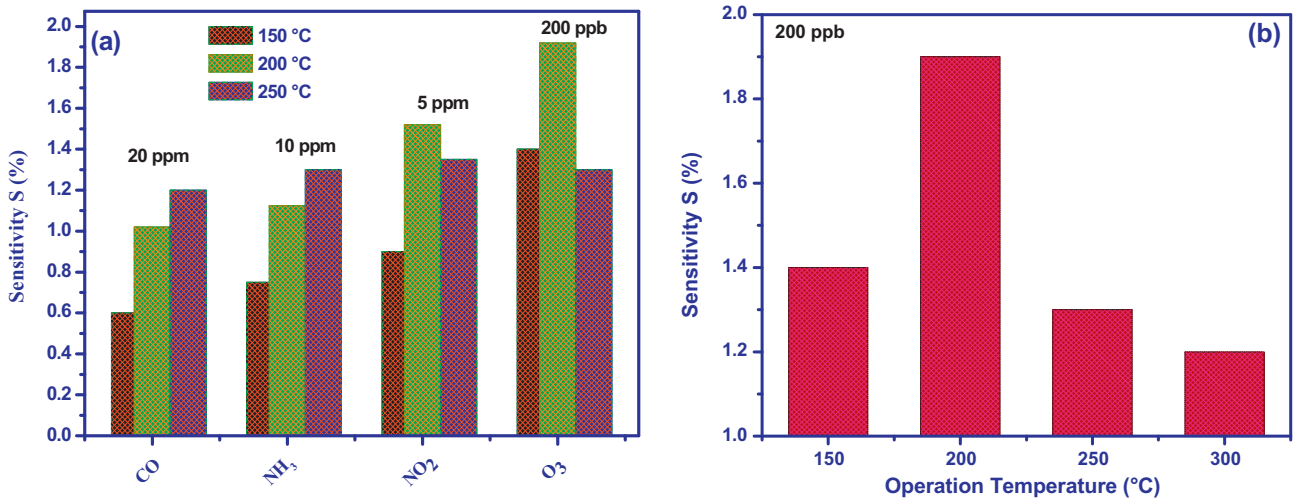

Fig. 6. (a) Oxidation (NO_2 and O_3) and reduction (CO and NH_3) gas sensing response, (b) the response to 200 ppb ozone gas (O_3) at different working temperatures for $CuAlO_2$ microspheres constituted of nanoparticles.

directly proportional to the gas sensitivity of the nanostructure materials because larger surface area results in larger contact area with the gaseous species. This demonstrates the importance of the surface area in gas-sensing application [35]. Specific surface area of $CuAlO_2$ microsphere constituted of nanoparticles was found to be 66.80 $m^2 g^{-1}$, using nitrogen adsorption–desorption isotherm through BET analysis. The sensing mechanism relies on the interaction between the dominating adsorbed molecular or atomic–ionic species (adsorbates) and the semiconductor surface. It is well known that morphology, size and surface area of nanostructure can dramatically enhance the sensor and catalytic applications of TCO materials [36]. So, it could be expected that the as-fabricated $CuAlO_2$ microsphere constituted of nanoparticles might be a potential candidate for toxic gas sensing applications. To investigate the toxic gas sensing application of the as-fabricated $CuAlO_2$ microspheres tests were performed towards several common reductive organic polluting gases such as oxidation (O_3 and NO_2) and reduction (NH_3 and CO). Fig. 6a displays $CuAlO_2$ microspheres exhibiting a significantly enhanced response to four different tested gases at different temperature. It can be observed from the figure that $CuAlO_2$ microspheres based sensor shows high response ~1.94 for very low ozone gas concentration (200 ppb). For other gases, it is as follows; response of 1.52 for 5 ppm NO_2, response of 1.12 for 10 ppm NH_3 and CO was detectable for high concentration of 20 ppm at low sensitivity of 0.98 at 200 °C. The process involved can be understood by considering the conduction mechanism of $CuAlO_2$ microspheres. The delafossite-type $CuAlO_2$ microspheres usually show p-type conduction due to the defects of oxygen interstitials, Cu vacancies and unsaturated bonds which are introduced by the non-stoichiometric of the materials [37]. When the $CuAlO_2$ was exposed to ozone gas, ppb level of ozone gas get absorbed on to the surface, because of the larger electron affinity of O_3 molecule (2.103 eV), which would act as unsaturated bonds that can accept electrons and enrich hole concentration on $CuAlO_2$ surface. Thus, ozone sensing of $CuAlO_2$ samples is due to additional hole concentration in their surface enriched region in the presence of ozone. These explain the better sensing features of $CuAlO_2$ microsphere sensors when compared to other gases.

Further, it reveals that the sensor based on $CuAlO_2$ microspheres shows an obvious advantage in selective detection of ozone at 200 ppb, without any interference from other common oxidation and reducing gases because of high detection level (ppb). We also find a different resistance change between oxidation (O_3, NO_2) and reducing gases (CO, NH_3) on the p-type $CuAlO_2$ sensor surface: the change in resistance is negative for oxidizing gases and positive for reducing gases. The reason could be when oxygen molecules are absorbed onto the surface of p-type $CuAlO_2$ microspheres, they obtain electrons from the material and form (O^-, O_2^-), resulting in the formation of hole accumulation layers on the surface of the materials after the chemisorption process reaches equilibrium. For oxidation gases, such as O_3 and NO_2, it adsorbs on the $CuAlO_2$ sensor surface, capture the electrons from the surface of $CuAlO_2$ microspheres, causing the decrease in resistance or increase of electric conductivity. However, for CO, NH_3, the measured gas molecules react with the absorbed oxygen molecules, leading to the release of electrons back to the materials, causing increase resistance or decrease conductivity. Therefore, difference in resistance between oxidation and reducing gases exists. Further, the selectivity of the sensor to ozone concentration was nearly 50 (NH_3) and 100 (CO) times greater than the reducing vapours and approximately 25 times greater than NO_2. The most desirable ozone sensor would be one which is sensitive to only a single gas and is not affected by any other gases. Therefore, the good selectivity to target gas is always one of the key factors to the gas sensors. Hence, in the present study ozone gas detection at 200 ppb level was measured. Fig. 6b shows the response of the sensor towards 200 ppb of ozone gas examined as a function of operating temperature in the range 150–300 °C from which the optimum operating temperature was determined. It is obviously observed that for gas responses of $CuAlO_2$ microsphere sensors with an increase in operating temperature, the response increases at first (150 and 200 °C), reaches a maximum at 200 °C and finally drops at 250 and 300 °C. The reason could be, the reaction between tested gas molecules and the surface of metal oxides involves an adsorption–desorption kinetics process that is heavily dependent on the operation temperature [38]. Therefore, the operating temperature of 200 °C was fixed as optimum working temperature to proceed with further analysis.

Fig. 7a shows the dynamic response–recovery curves of the sensor based on the $CuAlO_2$ microspheres upon exposure to the three kinds of ozone gas concentrations 200, 600 and 1150 ppb in the background of dry air, at a working temperature of 200 °C. From the results, it can be clearly observed that the output signal

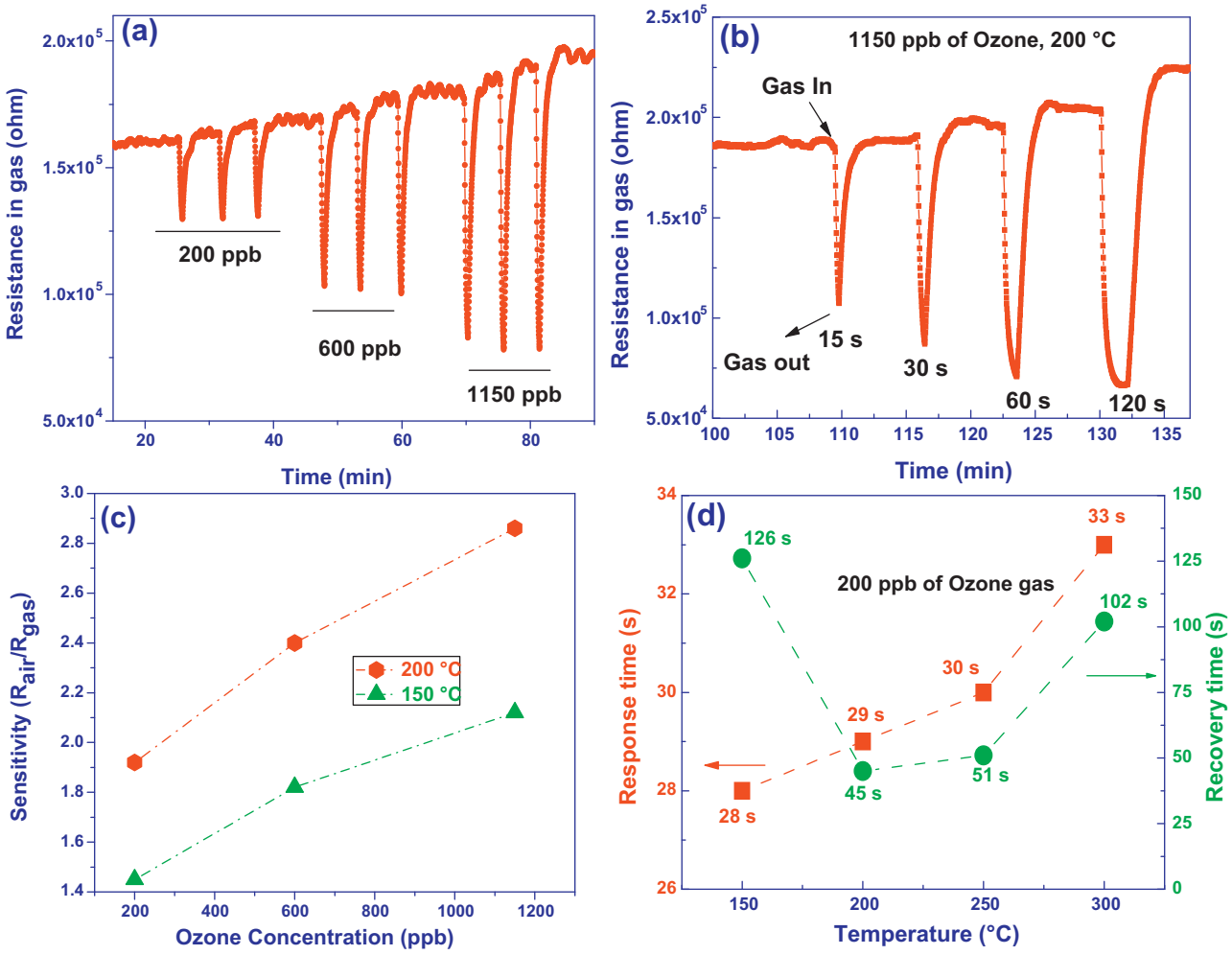

Fig. 7. (a) Response and recovery transients of the sensor with different ozone gas concentration, (b) different ozone gas flow time at 200 °C (arrows indicate when the ozone gas flow was in and out), (c) dependence of response on the ozone concentration at operating temperature 150 and 200 °C and (d) response and recovery time (s) of the statistical reports of $CuAlO_2$ microspheres.

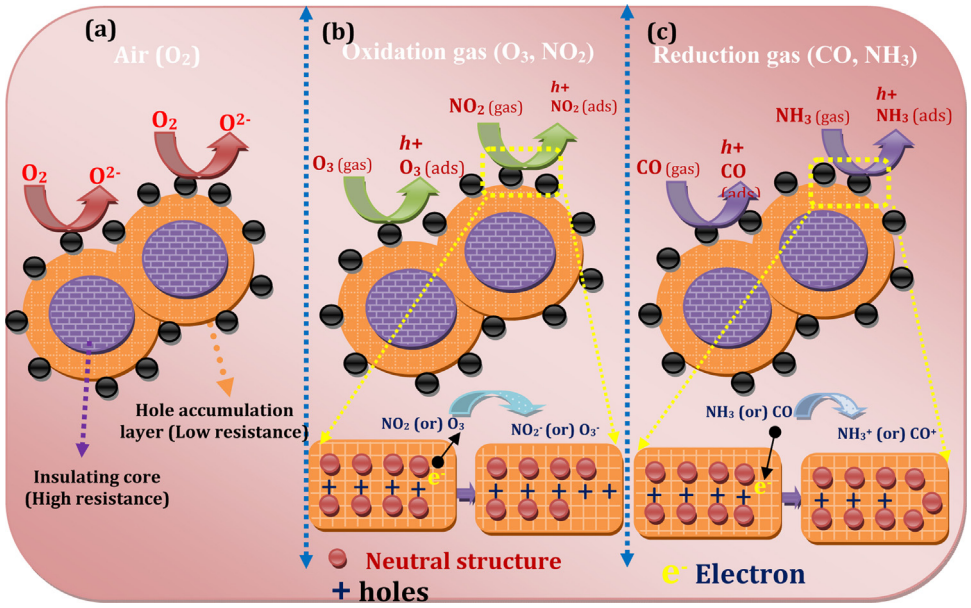

Fig. 8. Schematic diagrams for oxidation (O_3 and NO_2) and reducing (CO and NH_3) type gas sensing operating mechanism on p-type $CuAlO_2$ microspheres constituted of nanoparticles.

resistance of the sensor decreases dramatically for the ozone gas, then increases and recovers to the initial value after the ozone gas is released, indicating the p-type response of the $CuAlO_2$ microsphere based ozone sensor. It can also be seen that the response amplitudes of the sensor increase on increasing the test gas concentration, and the sensor shows remarkable signal change upon exposure to all concentration of ozone gas. In addition, ozone gas sensor response of $CuAlO_2$ microspheres to three different concentrations was tested for three repeated cycles. The sensor maintains the initial response amplitude without a clear decrease upon three successive sensing tests to the same concentration of ozone. When compared with the original response values for the same concentrations the sensor only shows a slight deviation in the response values, which reveals the good reproducibility and stability of the as-fabricated $CuAlO_2$ microsphere sensor.

Further, Fig. 7b shows the dynamic gas-sensing characteristics of $CuAlO_2$ microsphere based sensor exposed to 1150 ppb ozone (O_3) gas with different gas flow time 15, 30, 60 and 120 s in the background of dry air. The operating temperature maintained was 200 °C. The four different exposure time were carried out in an on-and-off process. When O_3 gas was introduced, the resistance of $CuAlO_2$ microsphere sensor decreases obviously. While ozone gas was shut, the resistance increases and reaches initial position again. The present $CuAlO_2$ microspheres exhibit good sensitivity to the different exposure time as well as total reversibility and good stability of the base line. Sensitivity is an important factor for toxic gases, a higher sensitivity usually results in a low detection limit.

Fig. 7c displays the ozone gas sensing performance of $CuAlO_2$ microspheres for different working temperature 150 and 200 °C and different ozone concentration. It is clear that both working temperature, ozone concentration (200–1150 ppb) increase with sensitivity (1.92–2.89) and greater sensitivity is observed at 200 °C. So, we consider best optimum working temperate as 200 °C and low ozone concentration as 200 ppb. Response and recovery time are the very important parameters of a toxic gas sensor. In semiconductor gas sensor, at certain operating temperature, the recovery time is usually longer than response time.

The dependence of response and recovery time of the $CuAlO_2$ microsphere based sensors to 200 ppb of ozone gas at different operating temperature with an experimental error of ±0.01% are shown in Fig. 7d. At working temperature 150, 250 and 300 °C the response was 28, 30, and 33 s with high recovery time (126, 51 and 102 s), while at 200 °C the response was found to be 29 s and shorter recovery time of 45 s. It is obvious that the response and recovery time decrease with increasing the operating temperature. Hence, at low temperature of 150 °C, the adsorbed ozone molecules are not activated enough to overcome the activation energy barrier to react with the adsorbed oxygen species, while at high temperatures (250 and 300 °C) the gas adsorption is too difficult to be adequately compensated for by the increased surface reactivity. But, fast response and recovery behaviour was observed at 200 °C, which indicates the activation energy of adsorption–desorption and thereby the kinetics of surface chemisorption reaction on the $CuAlO_2$ microspheres is strong due to the low concentration (200 ppb). On the other hand, the recovery time of $CuAlO_2$ sensing sample is shorter than other reported p and n-type ozone gas sensors [39,18,40–42]. Thus, we confirm that the response of the fabricated $CuAlO_2$ microsphere sensors towards ozone gas strongly depends on the operating temperature as well as the concentration of test gas. Finally, the above results clearly demonstrate the great advantage of employing $CuAlO_2$ microspheres constituted of nanoparticles for real-time monitoring of ozone gas sensor for 200 ppb detection level at 200 °C.

3.7. Gas sensing mechanism and charge transport properties of $CuAlO_2$ microspheres

At a typical surface-based reaction, the sensor response greatly depends on the morphology, size, structure, and exposed crystal surfaces of the toxic sensing materials. The sensing mechanism mainly includes the gas adsorption, charge transfer, and desorption process. p-Type semiconductors increases (or decreases) when oxidizing (or reducing) gases are adsorbed on their surface (opposite for n-type semiconductors) [43]. In p-type semiconducting oxide, adsorbed oxygen behaves as a surface acceptor state, trapping electrons from the valence band and hence increasing the hole concentration. In general case, the interaction of oxidation with the adsorbed oxygen at the sensor surface has been explained in our previous publication [44].

The adsorption of oxygen anions in p-type oxide semiconductors form the hole accumulation layers (HAL) near the surface of the material because of the electrostatic interaction between the oppositely charge species, which again establishes the electronic core–shell configuration; that is, the insulating region at the cores of particles and semiconducting HALs near the surface of the particles [44].

The different gas-sensing behaviour combined with the gas sensing mechanism of the $CuAlO_2$ microspheres constituted of nanoparticles can be examined in detail from Fig. 8 $CuAlO_2$ is a p-type semiconductor, the acceptor level lies near the valance band and at operating temperature all the acceptor levels are ionized (filled) leaving holes in the valance band, the $CuAlO_2$ ion vacancies are the acceptors. When operated at a moderate temperature, the oxygen molecules in air can trap electrons from the $CuAlO_2$ conduction band and form chemisorbed oxygen species (O_2^-, O^-, and O^{2-}) on the surface of the sensing layer, which has been represented in the following equation, i.e. the adsorption of negatively charged oxygen can generate the holes.

$$O_2\,(\text{gas}) \Longleftrightarrow O_2\,(\text{ads}) + h^+ \Longleftrightarrow O_2^-\,(\text{ads}) + h^+ \Longleftrightarrow 2O^-\,(\text{ads}) + h^+ \Longleftrightarrow O^{2-}\,(\text{ads}) + h^+ \quad (1)$$

When oxidation gas ozone (O_3) and NO_2 are introduced to the surface of $CuAlO_2$ samples as shown in Fig. 8b, the ozone or NO_2 molecules adsorb on the $CuAlO_2$ surface acting as acceptors. This surface trapping of lone-pair electrons causes band bending which results in the formation of free holes and an increase in hole concentration near the interface forming the hole accumulated layer at the $CuAlO_2$ surface which decrease the resistance of $CuAlO_2$ samples. The following reaction (Eq. (2)) takes place on the surface of $CuAlO_2$ sensing film for oxidation gases.

$$CuAlO_2 + O_3 \text{ or } NO_2\,(gas) \rightleftharpoons CuAlO_2^{+} - O_3^{-} \text{ or } NO_2^{-}(ads) \rightarrow CuAlO_2 - O_3^{-}(ads) \text{ or } NO_2^{-}(ads) + h \quad (2)$$

Further, the accepted electrons in the reactions are annihilated with neutral structure (Eq. (3)) and same reaction has been represented in the schematic diagram shown in Fig. 8b (bottom).

$$e^{-} + \bullet \rightleftharpoons + \quad (3)$$

Then, for p-type semiconductors, oxygen adsorption produces an increase in the number of holes in the valence hand, which increases their conductivity [45]. When the sensor was exposed to the reducing gases such as CO and NH_3 at 200 °C, the interaction between the reducing gas and the adsorbed oxygen ions on the $CuAlO_2$ sensors surface can be explained as:

$$CuAlO_2 + CO \text{ or } NH_3\,(gas) \rightleftharpoons CuAlO_2^{+} - CO^{+} \text{ or } NH_3^{+}\,(ads) \rightarrow CuAlO_2 - CO^{+} \text{ or } NH_3^{+}\,(ads) + h \quad (4)$$

The released electrons in the reactions are annihilated with holes (Eq. (5)) and have been represented in the schematic diagram as shown in Fig. 8c (bottom).

$$\text{Hole } (+) + e^{-} \rightleftharpoons \text{null} \quad (5)$$

Electrons are injected into the conduction band and then coupled with holes in the valence band, producing a decrease in the conductivity or increased resistance. This change in the conductivity indicates that the examined $CuAlO_2$ microspheres sample posses a typical p-type semiconducting feature. In addition, HAL emerge as oxygen molecules absorb to the surface of the materials. These HAL may overlap with each other along the producing continuous hole transfer channels. Other hand, interestingly, $CuAlO_2$ oxides were found to have enhanced sensing characteristics for a complex molecular structure or a reactive functional group of ozone gas. These may be reason for the low detection of ozone gas in our present $CuAlO_2$ surface compared to other gases. The result suggests that the prepared $CuAlO_2$ microspheres have superior (200 ppb) gas sensing property and is a promising candidate for good performance ozone gas sensor for environmental remediation.

4. Conclusion

In summary, novel ozone gas sensing material $CuAlO_2$ microspheres were successfully prepared and the investigation on structural, morphology and effects of hydrothermal reaction time. In addition, the $CuAlO_2$ microsphere based sensor showed excellent linear response to ozone gas concentrations in the range 200–1150 ppb, with good reproducibility, short response–recovery time (29/45 s), and good response. These results are found to be better than other reported oxidation and reduction gases. The improved ozone sensing properties was also briefly explained in gas sensing mechanism due to charge transport properties and morphology effect. Finally, these results indicate that $CuAlO_2$ microspheres with excellent surface actives sites based toxic sensor is a real time monitoring and promising potential candidate for good performance at ppb-level ozone gas sensors.

Acknowledgements

The authors are gratefully acknowledge to the Brazilian research funding agency FAPESP (Process 2013/19049-0 and 2013/07296-2). The presented research was partially carried out at the LNLS, National Laboratory of Synchrotron Light, Brazil.

References

[1] D.P. Volanti, A.A. Felix, M.O. Orlandi, G. Whitfield, D.J. Yang, E. Longo, H.L. Tuller, J.A. Varela, The role of hierarchical morphologies in the superior gas sensing performance of CuO-based chemiresistors, Adv. Funct. Mater. 23 (2013) 1759–1766.
[2] C.S. William, E. Mugnier, A. Barnabe, J.M. Tobin, R.P. Kenneth, Hydrothermal synthesis of delafossite-type oxides, Chem. Mater. 18 (2006) 7–20.
[3] H. Kawazoe, M. Yasukawa, H. Hyodo, M. Kurita, H. Yanagi, H. Hosono, P-type electrical conduction in transparent thin films of $CuAlO_2$, Nature 389 (1997) 939–942.
[4] G. Thomas, Nature, materials science, Invis. Circuits 389 (1997) 907–908.
[5] S. Thirumalairjan, K. Girija, V.R. Mastealro, N. Ponpandian, Surface morphology-dependent room-temperature $LaFeO_3$ nanostructure thin films as selective NO_2 gas sensor prepared by radio frequency magnetron sputtering, ACS Appl. Mater. Interfaces 6 (2014) 13917–13927.
[6] H.M. Luo, M. Jain, T.M. McCleskey, E. Bauer, A.K. Burrell, Q.X. Jia, Optical and structural properties of single phase epitaxial p-type transparent oxide thin films, Adv. Mater. 19 (2007) 3604–3607.
[7] T.V. Thu, P.D. Thanh, K. Suekuni, N.H. Hai, D. Mott, M. Koyano, S. Maenosono, Synthesis of delafossite $CuAlO_2$ p-type semiconductor with a nanoparticle-based Cu(I) acetate-loaded boehmite precursor, Mater. Res. Bull. 46 (2011) 1819–1827.
[8] H. Yanagi, S. Inoue, K. Ueda, H. Kawazoe, H. Hosono, N. Hamada, Electronic structure and optoelectronic properties of transparent p-type conducting $CuAlO_2$, J. Appl. Phys. 88 (2000) 4159.
[9] S. Zhou, X. Fang, Z. Deng, D. Li, W. Dong, R. Tao, G. Meng, T. Wang, Room temperature ozone sensing properties of p-type $CuCrO_2$ nanocrystals, Sens. Actuators B 143 (2009) 119–123.
[10] V.R.M. Mastealro, C.Z. Sergio, L.F. Silva, I.P. Pedro, I.B. Maria, G. Jacques, A. Khalifa, Ozone gas sensor based on nanocrystalline $SrTi1–xFexO_3$ thin films, Sens. Actuators B 181 (2013) 919–924.
[11] O.S. David, W.W. Graeme, Conductivity limits in $CuAlO_2$ from screened-hybrid density functional theory, J. Phys. Chem. Lett. 1 (2010) 3195–3199.
[12] M. Shimode, M. Sasaki, K. Mukaida, Synthesis of the delafossite-type $CuInO_2$, J. Solid State Chem. 151 (2000) 16–20.
[13] Z. Deng, X. Zhu, R. Tao, W. Dong, X. Fang, Synthesis of $CuAlO_2$ ceramics using sol–gel, Mater. Lett. 61 (2007) 686–689.
[14] B.J. Ingram, G.B. Gonzalez, T.O. Mason, D.Y. Shahriari, A. Barnabe, D. Ko, K.R. Poeppelmeier, Transport and defect mechanisms in cuprous delafossites comparison of hydrothermal and standard solid-state synthesis in $CuAlO_2$, Chem. Mater. 16 (2004) 5616–5622.
[15] S. Thirualairajan, K. Girija, V. Ganesh, D. Mangalaraj, C. Viswanathan, N. Ponpandian, Shape evolution of perovskite $LaFeO_3$ nanostructures: a systematic investigation of growth mechanism, properties and morphology dependent photocatalytic activities, RSC Adv. 3 (2013) 7549–7561.

[16] K. Girija, S. Thirumalairajan, A.K. Patra, D. Mangalaraj, N. Ponpandian, C. Viswanathan, Enhanced photocatalytic performance of novel self-assembled floral β-Ga_2O_3 nanorods, Curr. Appl. Phys. 13 (2013) 652–658.
[17] T. Sato, K. Sue, H. Tsumatori, M. Suzukic, S. Tanaka, A.K. Nakamura, K. Saitohc, K. Aida, T. Hiaki, Hydrothermal synthesis of $CuAlO_2$ with the delafossite structure in supercritical water, J. Supercrit. Fluids 46 (2008) 173–177.
[18] N. Tsuboi, Y. Takahashi, S. Kobayashi, H. Shimizu, K. Kato, F. Kaneko, Delafossite $CuAlO_2$ films prepared by reactive sputtering using Cu and Al targets, J. Phys. Chem. Solids 64 (2003) 1671–1674.
[19] G. Korotcenkov, B.K. Cho, Ozone measuring: what can limit application of SnO_2-based conductometric gas sensors, Sens. Actuators B 161 (2012) 28–44.
[20] G. Korotcenkov, I. Blinov, M. Ivanov, J.R. Stetter, Ozone sensors on the base of SnO_2 films deposited by spray pyrolysis, Sens. Actuators B 120 (2007) 679–686.
[21] J. Smith, T. Van Steenkiste, X.G. Wang, Thermal photocatalytic generation of H_2 over $CuAlO_2$ nanoparticle catalysts in H_2O, Phys. Rev. B: Condens. Matter Mater. Phys. 79 (2009) 041403.
[22] C. Baratto, M. Ferroni, G. Faglia, G. Sberveglieri, Iron-doped indium oxide by modified RGTO deposition for ozone sensing, Sens. Actuators B 118 (2006) 221–225.
[23] J. Brunet, V. Parra Garcia, A. Pauly, C. Varenne, B. Lauron, An optimised gas sensor microsystem for accurate and real-time measurement of nitrogen dioxide at ppb level, Sens. Actuators B: Chem. 134 (2008) 632–639.
[24] L. Ankudinov, B. Ravel, S.D. Conradson, J.J. Rehr, Real-space multiple-scattering calculation and interpretation of X-ray-absorption near-edge structure, Phys. Rev. B: Condens. Matter Mater. Phys. 58 (1998) 7565.
[25] H. Yoo, J. Sharma, J.K. Kim, A.P. Shreve, J.S. Martinez, Tailored microcrystal growth: a facile solution-phase synthesis of gold rings, Adv. Mater. 23 (2011) 4431–4434.
[26] J. Hu, K. Zhu, L. Chen, H. Yang, Z. Li, A. Suchopar, R. Richards, Preparation and surface activity of single-crystalline NiO(1 1 1) nanosheets with hexagonal holes: a semiconductor nanospanner, Adv. Mater. 20 (2008) 267–271.
[27] J.C. Love, L.A. Estroff, J.K. Kriebel, R.G. Nuzzo, G.M. Whitesides, Self-assembled monolayers of thiolates on metals as a form of nanotechnology, Chem. Rev. 105 (2005) 1103–1170.
[28] S. Thirumalairjan, K. Girija, V.R. Mastealro, N. Ponpandian, Photocatalytic degradation of organic dyes under visible light irradiation by floral-like $LaFeO_3$ nanostructures comprised of nanosheet petals, New J. Chem. 38 (2014) 5480–5490.
[29] R.H. Jarman, J. Bafiaa, T. Gebreslasse, B. Ingram, J. David Carter, Synthesis of the p-type semiconducting ternary oxide $CuAlO_2$ using the pechini method, Mater. Res. Bull. 48 (2013) 3916–3918.
[30] K. Girija, S. Thirumalairajan, G.S. Avadhani, D. Mangalaraj, N. Ponpandian, C. Viswanathan, Synthesis, morphology, optical and photocatalytic performance of nanostructured β-Ga_2O_3, Mater. Res. Bull. 48 (2013) 2296–2303.
[31] J. Ahmed, C.K. Blakely, J. Prakash, M. Yu, Y. Wu, V.V. Poltavets, Scalable synthesis of delafossite $CuAlO_2$ nanoparticles for p-type dye-sensitized solar cells applications, J. Alloys Compd. 591 (2014) 275–279.
[32] K.T. Jacob, C.B. Alcock, Thermodynamics of $CuAlO_2$ and $CuAl_2O_4$ and phase equilibria in the system Cu_2O–CuO–Al_2O_3, J. Am. Ceram. Soc. 58 (1975) 192–195.
[33] D. Bazin, J.J. Rehr, Limits and advantages of X-ray absorption near edge structure for nanometer scale metallic clusters, J. Phys. Chem. B 107 (2003) 12398.
[34] F. Bridges, L. Downward, J.J. Neumeier, T.A. Tyson, Detailed relationship between local structure, polarons, and magnetization for La1–xCa$x$$MnO_3$ ($0.21 \leq x \leq 0.45$), Phys. Rev. B 81 (2010) 184401.
[35] H. Yoon, J.Y. Hong, J. Jang, Charge-transport behavior in shape-controlled poly(3,4-ethylenedioxythiophene) nanomaterials: intrinsic and extrinsic factors, Small 3 (2007) 1774.
[36] S. Thirumalairjan, V.R. Mastealro, C.A. Escanhoela Jr., In-depth understanding of the relation between $CuAlO_2$ particle size and morphology for ozone gas sensor detection at a nanoscale level, ACS Appl. Mater. Interfaces 6 (2014) 21739–21749.
[37] J. Tate, H.L. Ju, J.C. Moon, A. Zakutayev, A.P. Richard, J. Russell, D.H. McIntyre, Origin of p-type conduction in single-crystal $CuAlO_2$, Phys. Rev. B 80 (2009) 165206.
[38] Y. Zhang, J.Q. Xu, Q. Xiang, H. Li, Q.Y. Pan, P.C. Xu, Brush-like hierarchical ZnO nanostructures: synthesis, photoluminescence and gas sensor properties, J. Phys. Chem. C 113 (2009) 3430–3435.
[39] X.G. Zheng, K. Taniguchi, A. Takahashi, Y. Liu, C.N. Xu, Room temperature sensing of ozone by transparent p-type semiconductor $CuAlO_2$, Appl. Phys. Lett. 85 (2004) 1728–1729.
[40] H. Nakagawa, S. Okazaki, S. Asakura, H. Shimizu, I. Iwamoto, A new ozone. Sensor for an ozone generator, Sens. Actuators B 77 (2001) 543–547.
[41] J. Guerin, K. Aguir, M. Bendahan, Thermal modelling of a WO_3 ozone sensor response, Sens. Actuators B 104 (2005) 289–293.
[42] E. Gagaoudakis, M. Bender, E. Douloufakis, The influence of deposition parameters on room temperature ozone sensing properties of InO_x films, Sens. Actuators B 80 (2001) 155–161.
[43] M. Bender, E. Gagaoudakis, Production and characterization of zinc oxide thin films for room temperature ozone sensing, Thin Solid Films 418 (2002) 45–50.
[44] P. Song, H. Zhang, D. Han, J. Li, Z. Yang, W. Qi, Preparation of biomorphic porous $LaFeO_3$ by sorghum straw biotemplate method and its acetone sensing properties, Sens. Actuators B 196 (2014) 140–146.
[45] H.J. Kim, J.H. Lee, Highly sensitive and selective gas sensors using p-type oxide semiconductors: overview, Sens. Actuators B 192 (2014) 607–627.

Biographies

S. Thirumalairajan received his Ph.D. degree in Physics – Nanoscience and Technology (interdisplanery) from Bharathiar University, Coimbatore, India in the year 2013. He is currently working as FAPESP – post doctoral fellow in the Institute of Physics, University of Sao Paulo, Sao Carlos, Brazil. His research interests are on developing new techniques to prepare size and morphologically different functional nanostructure and thin films. Also, systematic investigation on size and morphology dependent properties for energy, environmental and biological applications. He is the author of over 25 papers in international peer-reviewed journals.

Valmor R. Mastelaro is currently the associate professor at the Institute of Physics of São Carlos, University of Sao Paulo, Brazil. He received his doctorate in Science from University Paris XI (France) in 1992. His research interests mostly deals with structural characterization of inorganic materials by X-ray diffraction spectroscopy (XAS) and electrical properties of perovskite oxide based nanostructure and ceramic materials. He is the author of over 170 papers in international peer-reviewed journals.